Fast Neutron Diagnostics on MTF Compression Experiments

M. Hildebrand, S. Howard, S. Barsky

General Fusion Inc., Burnaby, British Columbia, Canada

60th Annual Meeting of the APS Division of Plasma Physics, Portland, Oregon, November 5-9, 2018 **CP11.00189**

Abstract

Measurement of DD fusion neutrons is a key diagnostic for magnetized target fusion (MTF) experiments being conducted at General Fusion (GF). When combined with other available diagnostics, the detection of DD fusion neutrons can provide strong constraints on a model of plasma evolution during compression, in particular, ion temperature and density. GF is conducting a series of compression experiments, referred to as Plasma Compression Small (PCS), of which 16 have been completed. Results from the two most recent, PCS15 and PCS16 are presented here (see accompanying GF overview poster).

Scintillators

PCS experiments are monitored for high-energy particle emission using hydrocarbon liquid scintillator systems of a variety of designs. Scintillator output is digitized at high resolution over the course of the compression shot using a set of Agilent DSO6034A scopes. GF uses liquid scintillator detectors made by Scionix. The scintillator array used for PCS includes three small detectors (volume = 0.83 L) and six larger detectors (3.5 L). The small detectors are model V94A, filled with EJ-309 fluid. The large detectors are model V150A, one of which is filled with EJ-309, the other five are filled with EJ-301. The scintillators are fixed in a variety of locations near the experiment, ranging from 1-3 m from center, indicated in yellow in the figure below. Eight of the nine scintillators are shielded with 1" of lead to shield gamma rays (not shown).

Nine SCIONIX scintillators

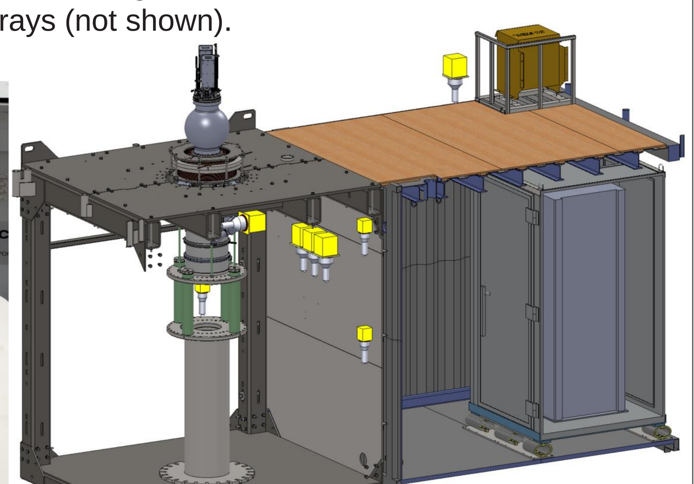

Location of scintillator array (yellow cubes)

EJ-301 (i.e. BC501A, NE213) is an older standard formulation of liquid hydrocarbon scintillator which provides good PSD separation between gamma rays and neutrons. EJ-309 is a newer formula that has less toxic additives, with a moderately reduced ability to do PSD on a mixed radiation field. Neutron pulse analysis is performed digitally using established methods, while each detector requires calibration with a γ source to determine the bifurcation curve between γ and n pulse shape parameters. The γ-based bifurcation curves have been verified for two scintillators with a neutron calibration using a DT neutron source.

Lead Shielding and Blast Protection

Neutron detection on PCS is complicated by several factors. There is an intrinsic issue with high energy photons (gammas, "γ") being produced by the plasma (possibly due to run-away electrons). Bursts of photon pulses can pile up and mask any coincident neutron pulses. Lead shielding is used to block most of the medium-low energy photons (E < 0.5 MeV) which seem to account for most of the pile-up bursts (see figure below). The lead shielding was cast into the space between a 3/16" inner and 1/4" outer mild steel casing (see pictures on right). The selected shielding thickness of 1" eliminates gammas with energy below 300 keV (see attenuation graph). This enclosure also provides protection against electromagnetic noise and impact from the compression blast.

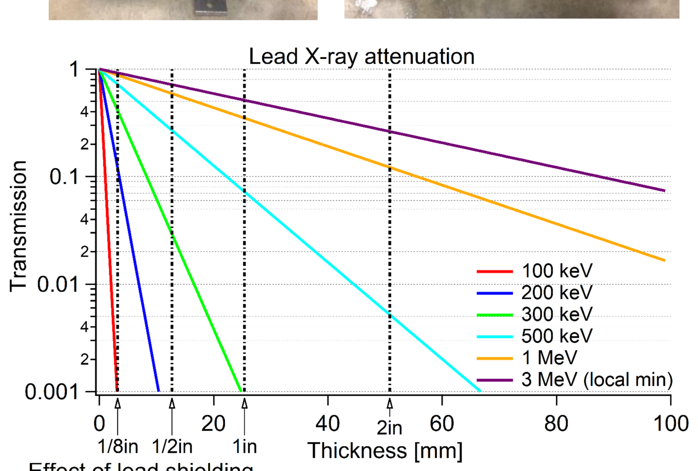

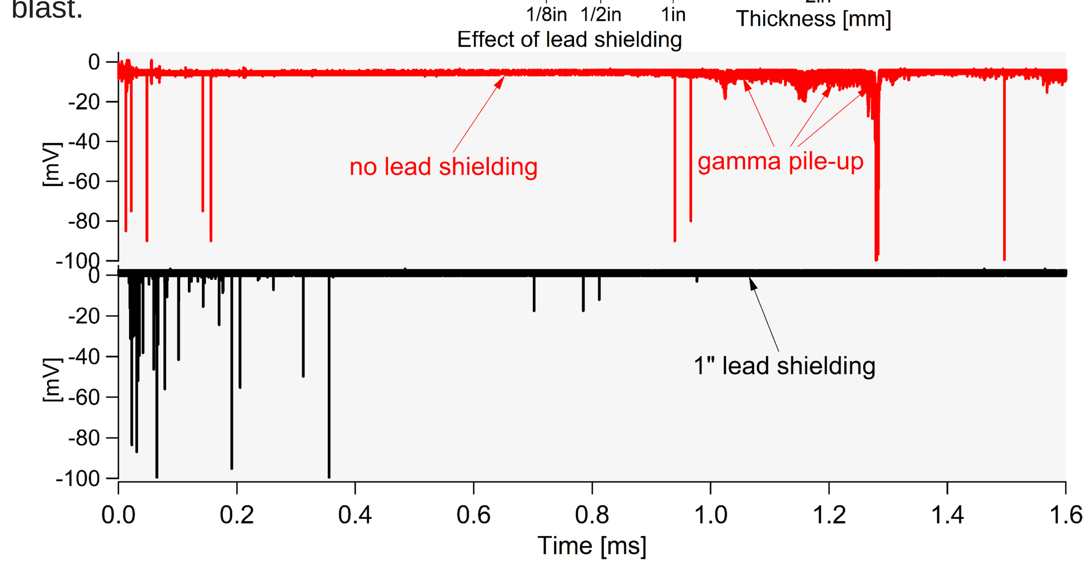

Pulse Shape Discrimination

The digitization of the signal from the scopes is followed by offline digital analysis of pulse height and shape of particle detection events. Neutron interactions in the scintillators have a brighter and quantifiably different decay then those from high-energy photons. An algorithm differentiates between the two by performing pulse shape discrimination (PSD). Pulses caused by neutron interactions have larger "tails" (see below figure) and can be differentiated from photon-initiated pulses by finding the ratio of their tail area divided by total area (see inset figure). A power law is fit to the γ data and used to bifurcate the pulse populations and identify neutrons and gamma rays (see right figure). The PSD algorithm also includes a number of steps to verify the integrity of pulses and ensure that no superimposed secondary pulses are present in the integrated areas.

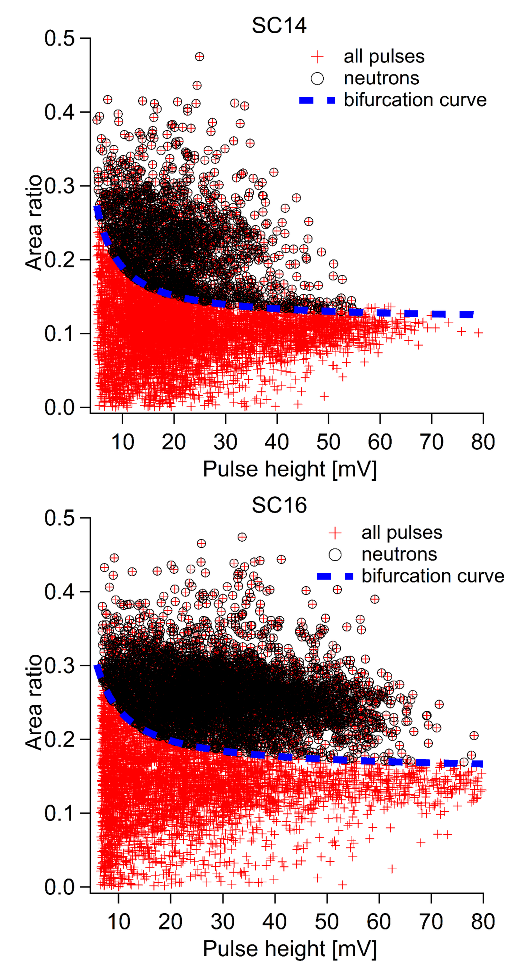

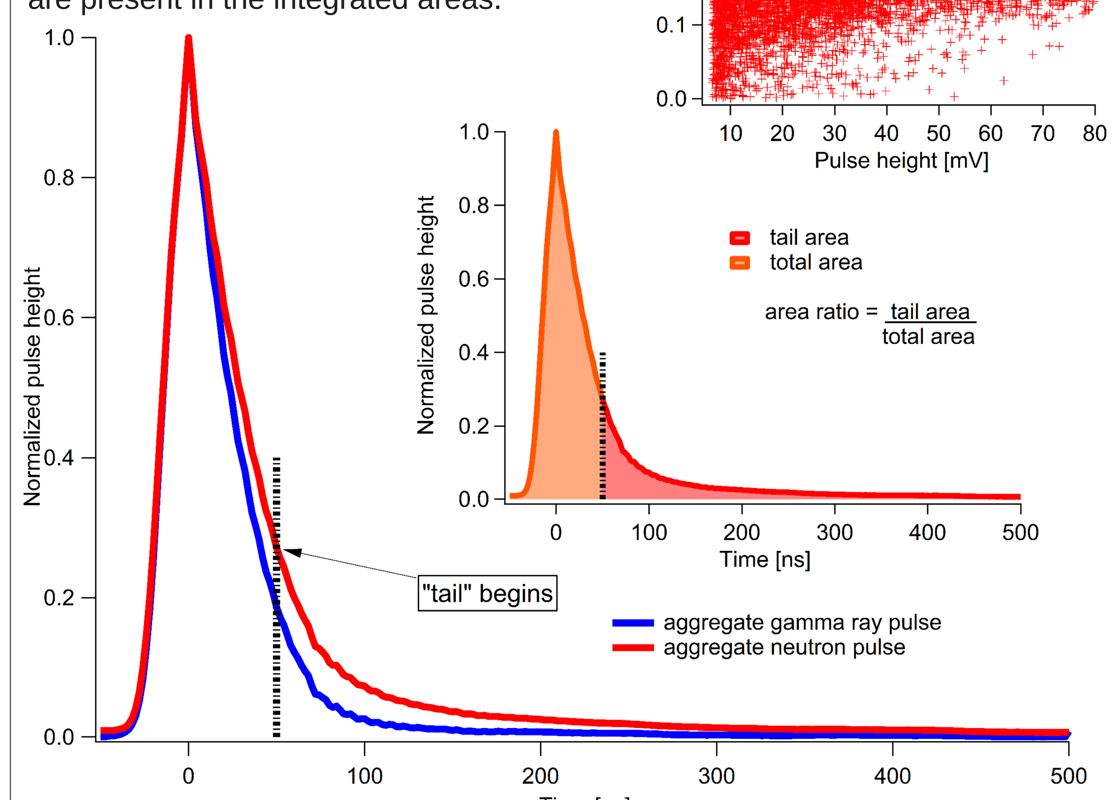

Calibration

Each detector is calibrated by observing γ emission from a 0.5 mCi Co-60 source, ($E\gamma$ = 1.17, 1.33 MeV). The pulse height spectrum of Compton scattered electrons gives a linear scaling between PMT pulse height in volts and incident γ energy in MeVee. This accounts for the variation in gain that exists between the different PMTs. The energy scaling for neutron detection is a nonlinear function of the γ-scaled energy of that pulse. This relationship is reported in various studies, and has been verified by DT neutron calibration with an incident energy of 14.1 MeV. Co-60 data is also used to find the bifurcation curve, defined as a power law fit to points representing the 95[th] percentile of gamma area ratios across a range of pulse heights. This bifurcation curve has also been verified with DT neutrons.

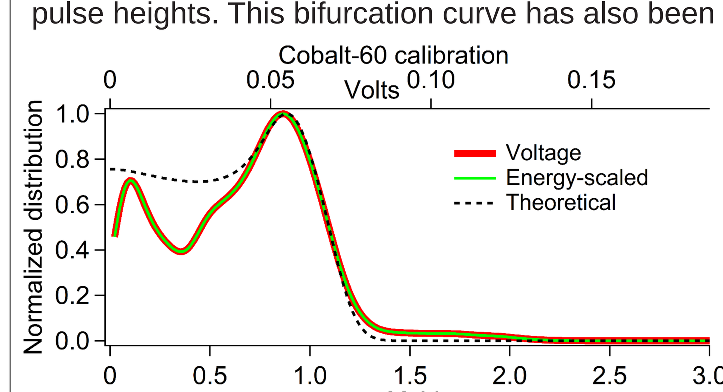

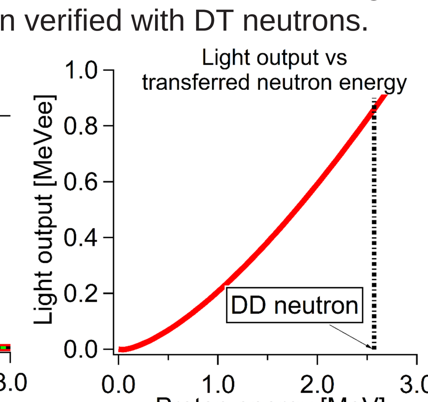

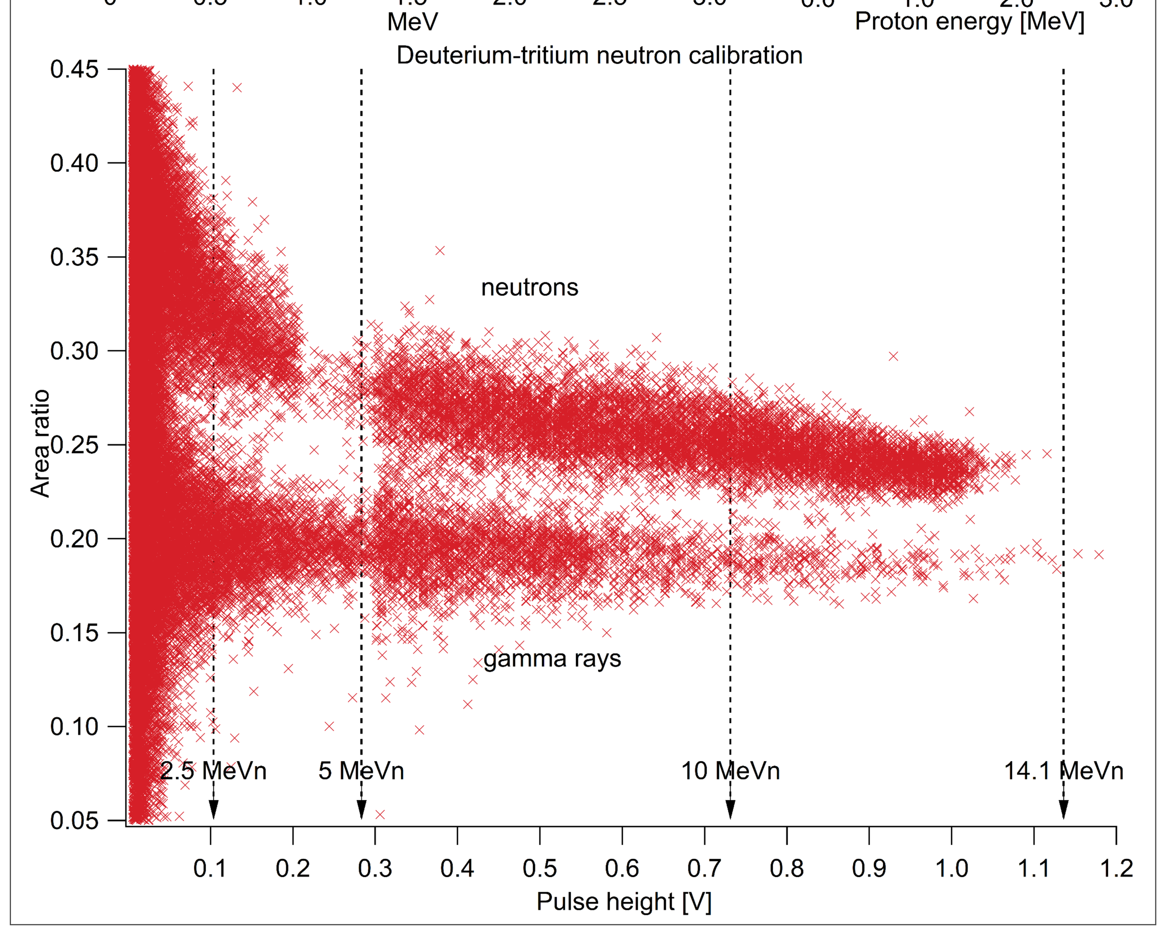

MCNP Simulations of Neutron Transport

MCNP is being used to model neutron and gamma transport on the PCS detector array geometry. The scintillators are modeled as a mixture of C and H that matches the atomic densities of the EJ-301 and EJ-309 liquids. The structure surrounding SPECTOR has been modelled along with the scintillators and their respective shielding. MCNP analysis tabulates the energy lost by each neutron upon its first collision within the scintillator, which can be compared to experimental, PSD-identified neutrons. The histograms below show the energy distribution of experimentally measured neutrons from lab plasma shots leading up to PCS16, compared to MCNP. The energy distributions computed by MCNP are based on a flux of DD neutrons applied to the structure, originating at the plasma's core location. At neutron energies above 1 MeV the experiment matches well with MCNP. At energies between 0.5 and 1 MeV the experimental counts decrease at lowering energies as the populations of neutrons and gamma begin to overlap on the area ratio vs. pulse height graphs (see PSD section). Neutrons with energies below 0.5 MeV cannot be experimentally differentiated from gammas due to this overlap.

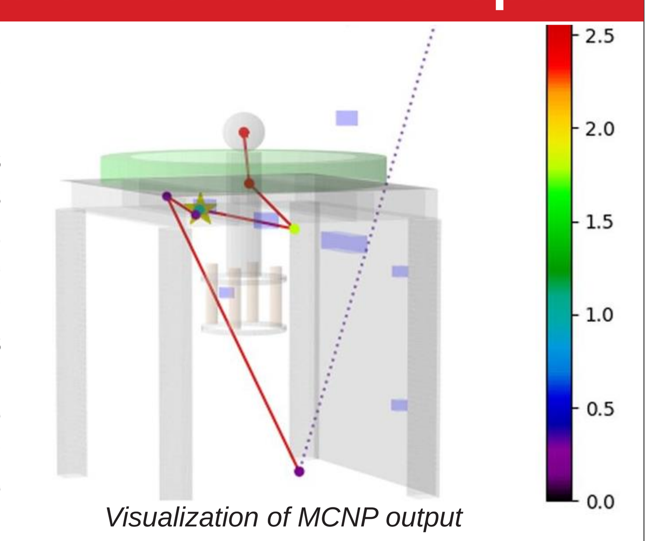

Visualization of MCNP output

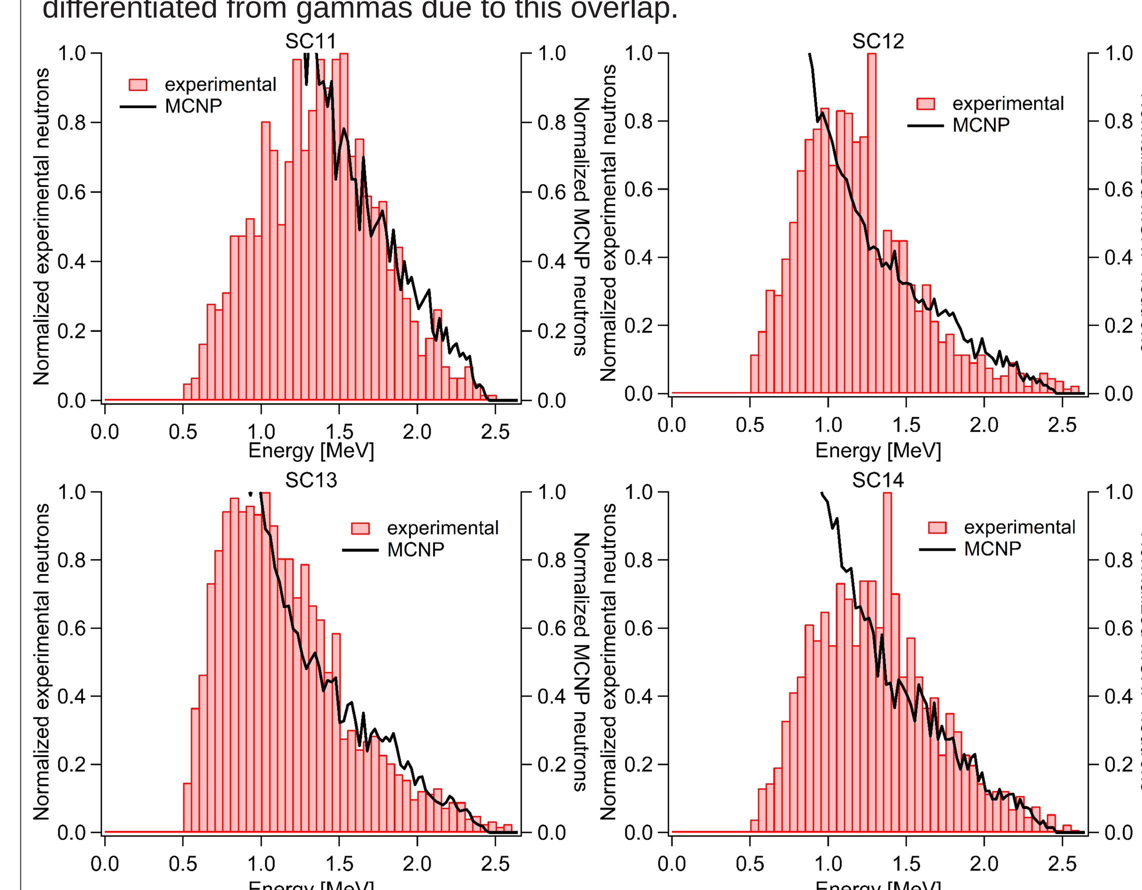

These energy spectra are used to determine the overall PSD efficiencies (η_{PSD}) of each scintillator. These efficiencies quantify the amount of neutrons at 0.5 < E < 1 MeV that cannot be differentiated from gammas by the PSD process. These are shown on inset graph, plotted against solid angle portion (normalized by 4π) of each scintillator. The relationship of η_{PSD} to solid angle is likely due to increased pileups at closer proximity. The scintillators that are closest to the experiment will experience more significant gamma ray flux, which will decrease the amount of PSD-detectable neutrons. The PSD efficiencies are extrapolated to lower energies to use MCNP along with experimental totals to predict the total flux of neutrons with energies exceeding 150 keV on each scintillator per shot. Below these MCNP-predicted totals are compared to experimental counts, as a function of solid angle portion. The experimental counts show a roughly linear relationship, with the scintillator above deck appearing as an outlier. Using MCNP results to augment the counts with undetectable neutrons, particularly at lower energies, removes this outlier. This comparison implies an approximate overall efficiency of 0.18.

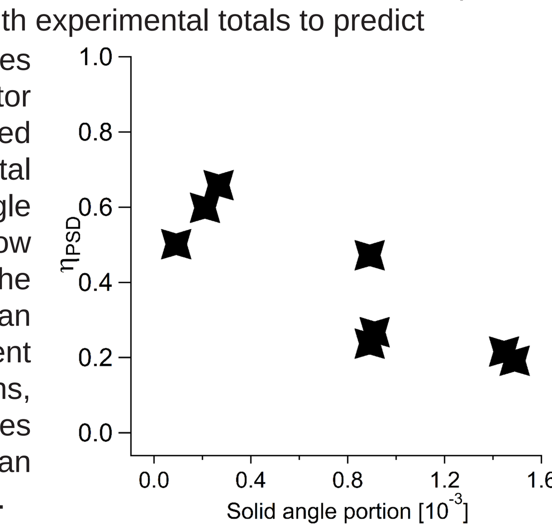

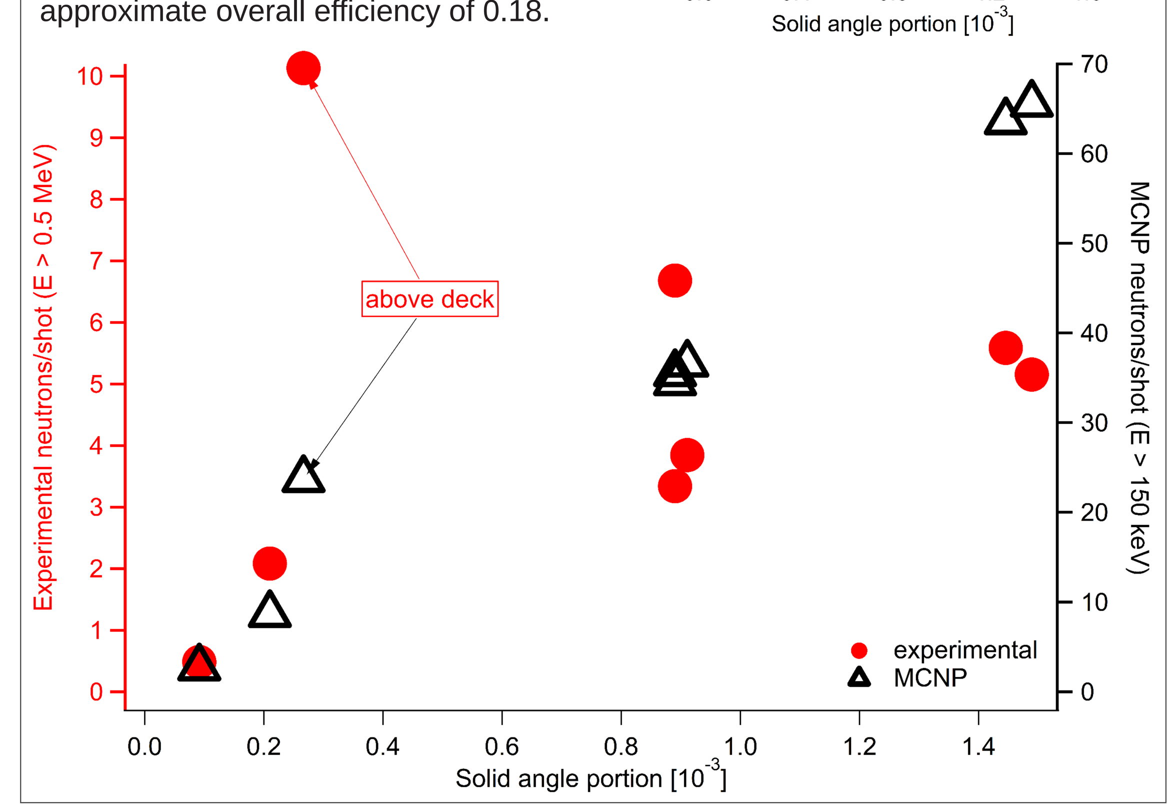

Compression Experimental Results

Neutron results from the two most recent compression experiments are shown here. The current array of nine scintillators was used for PCS16, while a smaller array of three was used for PCS15. Non-compressed lab shots using deuterium have a small background rate of neutrons. Therefore, it is necessary to compare neutron generation during compression to similar uncompressed shots to determine statistical significance. Shown below are graphs comparing PCS shots to a selection of similar shots taken directly before compression. The statistics are interpreted in 10 µs bins, the contours show σ envelopes corresponding to a bin-wise Poisson distribution assumption. The right axis indicates the precise probability of randomly measuring the number of neutrons counted during PCS in that time bin, given the background non-compression rate. For example, the burst of neutrons at t = 400 µs during PCS16 (lower graph) corresponds to two sequential events with probabilities of 3x10^{-6} (1 in 333,000).

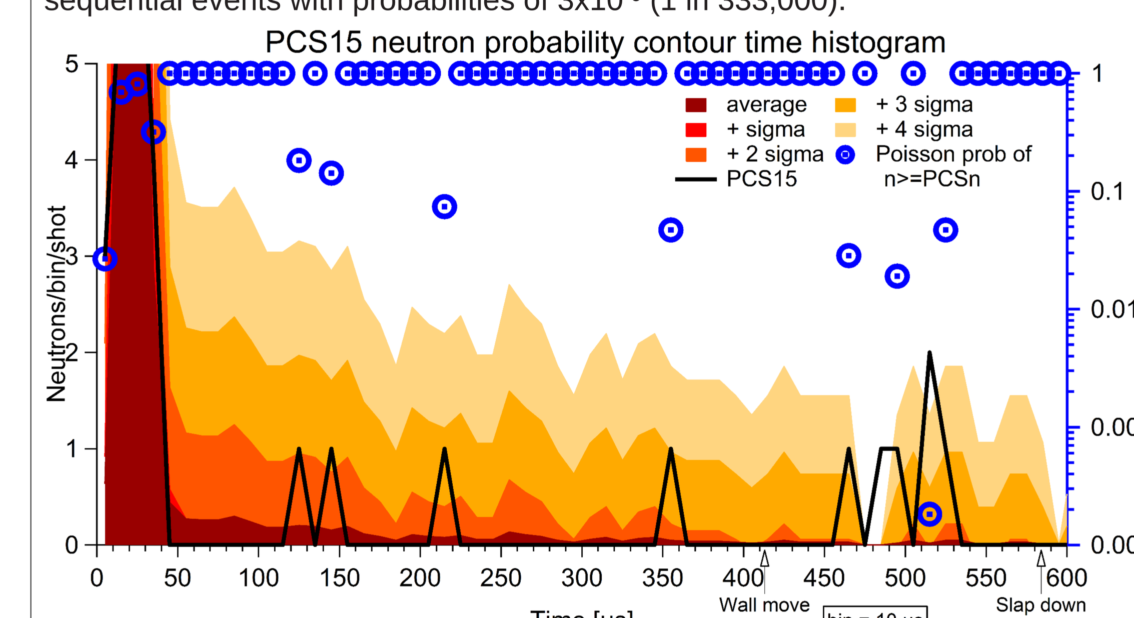

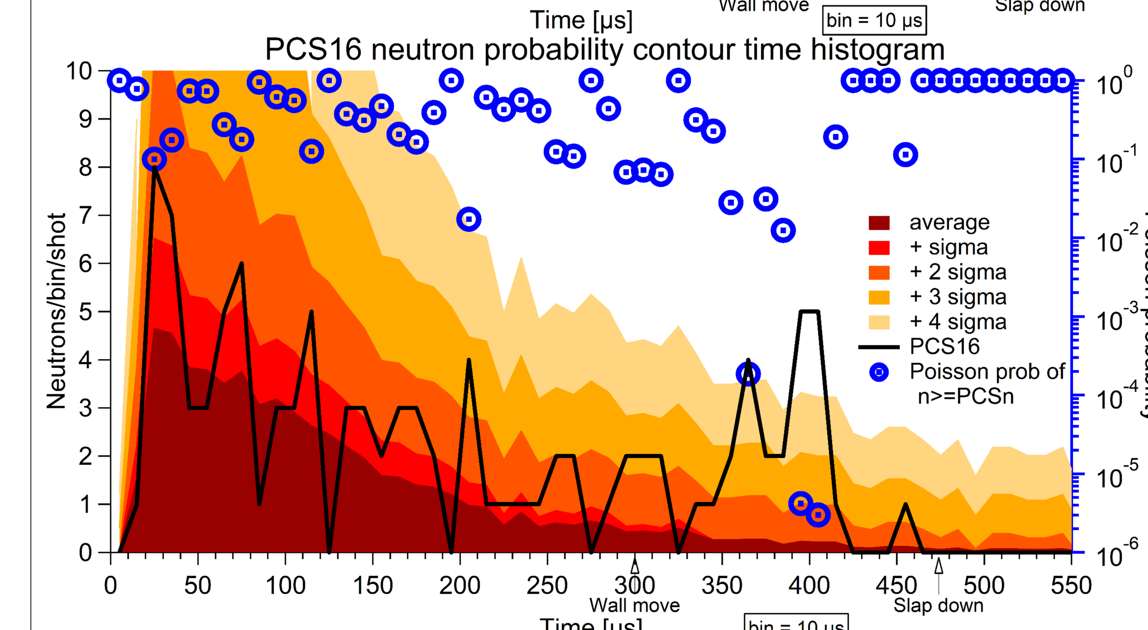

Analyzing the entire compression time window and comparing total compression neutron generation background rates from non-compression deuterium shots yields count histograms, shown below. PCS15 is compared to 105 such similar shots, PCS16 to 66. Overall array efficiencies were calculated using MCNP (see MCNP section). The results imply a total neutron yield of 12x10^4 for PCS15 and 8x10^4 for PCS16.

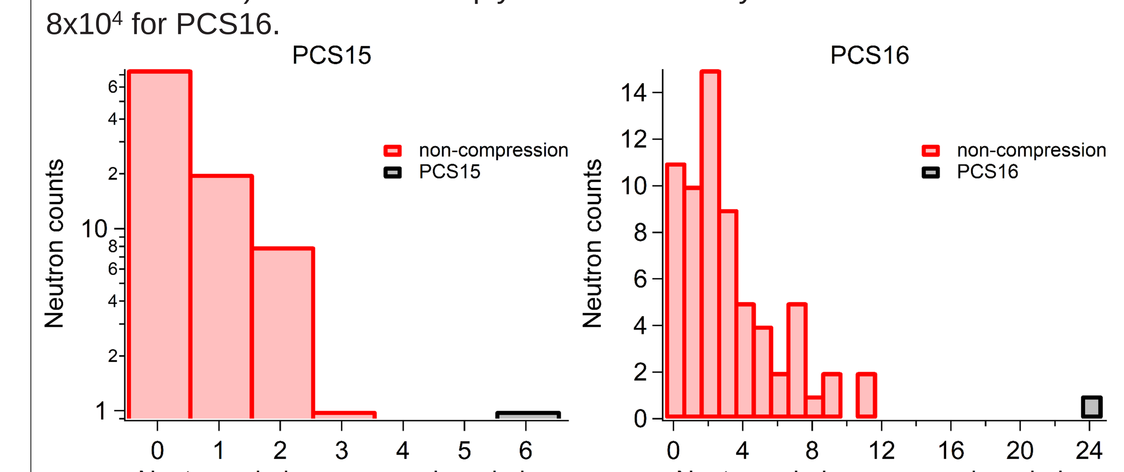

Inferred Ion Temperature

The scintillators do not suffer from line of sight issues (see GF overview poster) and are naturally weighted to the core ion temperature. Thus we have used our measurements of the neutron rate and the electron temperature to infer the core ion temperature, especially in our compressed plasmas.

$$\text{neutron rate}(n, T_i) = \int \frac{1}{2} n_i^2 \langle \sigma v(E_i) \rangle \, dV$$

As seen in the figure below, the inferred ion temperature during PCS16 rises from 700 to 790 eV during the first half of plasma compression.

PCS16 Compression Data